Determination of Size and Intensity Distribution of the Focal Spot of a Microfocus X-ray Tube Using Image Processing

Martin ENGELHARDT, Joachim BAUMANN, Siemens AG, Munich, Germany
Martin ENGELHARDT, Technische Universität München, Munich, Germany

Abstract. A novel technique for the determination of the intensity distribution of the focal spot of a microfocus X-ray tube is presented. An image of the focal spot is derived by evaluation of a projection image of a suitable test pattern using a standard image deconvolution algorithm. Using this method, the intensity distribution of focal spots with a spatial extent of a few micrometers can be measured. After an overview of existing methods and a discussion of mathematical foundations, the theoretical background of the novel approach is outlined, possible sources of error are discussed and first measurement results are presented which were acquired under normal industrial measurement conditions showing the intensity distribution of a focal spot with a spatial extent of a few microns.

1. Introduction

The spatial resolution of an X-ray setup is in general limited by the size of the focal spot and the point spread function of the detector system. Using nearly 1 : 1 imaging, the performance of the detector system is normally the dominating limiting factor for the spatial resolution, while using a higher magnification factor the size of the focal spot is the relevant limiting factor. For that reason, focal spot sizes down to or below 1 μm are applied in order to improve the spatial resolution. The size and optimally the intensity distribution of the focal spot at a given energy are therefore very important characteristic parameters of an X-ray tube. The determination of these parameters can be applied in order to compare and adjust X-ray tubes.

For medical applications relatively large focal spots with a typical size of more than 150 μm are used and the standards IEC 336 [1] and NEMA XR5 [2] can be applied. For nondestructive testing the norm DIN EN 12543 [3] can be used. Part 5 of this norm was designed to measure the size of focal spots of microfocus X-ray tubes, with a size between 5 μm and 300 μm, for X-ray energies up to 225 keV.

In order to measure the intensity distribution of the focal spot normally a pinhole is applied. However, difficulties can arise if the pinhole method is to be applied to a microfocus X-ray setup. The pinhole mask should be made out of a strongly absorbing material (e.g. tungsten with a thickness significantly higher than 100 μm for 50 keV X-rays) and the pinhole itself must have a size which is at least on the order of the focal spot.

A very promising approach is to determine size and shape of the focal spot by comparing the measurement result of a test object with a simulated measurement result. This idea was already proposed 1984 by J. Baumann [4]. It was outlined theoretically that the blurring of an acquired image can be described using the concept of image convolution and that it is possible to calculate the intensity distribution of the focal spot by inversion of this

convolution process using a division in Fourier space. The technique presented in the present paper is based on this idea. A new technique based on a similar idea was developed and applied successfully to focal spots with a spatial extent down to 3.3 μm at X-ray energies up to 100 kV by U. Taubenreuther [5]. A tungsten wire with a diameter of 10 μm was used as a test object. The parameters which determine the focal spot of a simulated measurement are varied until an optimal match between simulated and measured data is achieved. Another new technique based on the same principle was developed by A. Jobst et al. [6]. Here, a line pattern was applied as a test object.

2. The Novel Approach in Theory

2.1 Characterisation of Image Blurring in Microfocus X-ray Radiography Using Image Convolution

The processes which blur an acquired image can, under certain assumptions, be described mathematically using the concept of image convolution. The nomenclature which is used in this context is similar to that used in Barrett et al. [7].

The following assumptions are made:

- The transmission of the X-ray beam through a flat test object with its surface parallel to the surface of the detector system is measured. No X-rays are scattered by this object.
- The focal spot of the X-ray source is not point-like. It is extended in a plane which is parallel to the surface of the detector system.
- In addition to the extended focal spot of the X-ray tube, the detector system blurs the acquired images. It is assumed that this blurring process can be described mathematically as a convolution with the point spread function (PSF) of the detector system. In other respects the detector system is assumed to be ideal (after appropriate corrections).
- The acquired images are deteriorated by noise, which is relatively small compared to the image itself.

Fig. 1 shows the setup assumed and relates variables to the corresponding objects. The X-ray source, the flat object, and the intensity distribution measured at the detector system lie in different planes for which different coordinate systems with the variables (x, y), (x', y'), and (x'', y''), respectively, are used. This is done in order to include magnification effects in the calculations.

The result t of a measurement of the transmission of the X-ray beam through the flat test object for the setup assumed is to be derived mathematically. The measurement result can be calculated by convolving the normalized intensity distribution of the focal spot f with the transmission profile of the flat object g and the detector point spread function d. These functions are given in different planes, for which different coordinate systems are used, as shown in Fig. 1. In order to take into account the magnifying geometry of the setup, these functions are represented in one of these planes (here the plane of the detector), whereby the physical magnification effects of the setup were observed before the convolution is accomplished. Furthermore, t is deteriorated by noise, which is taken into consideration by addition of a noise term n to the result of the convolution.

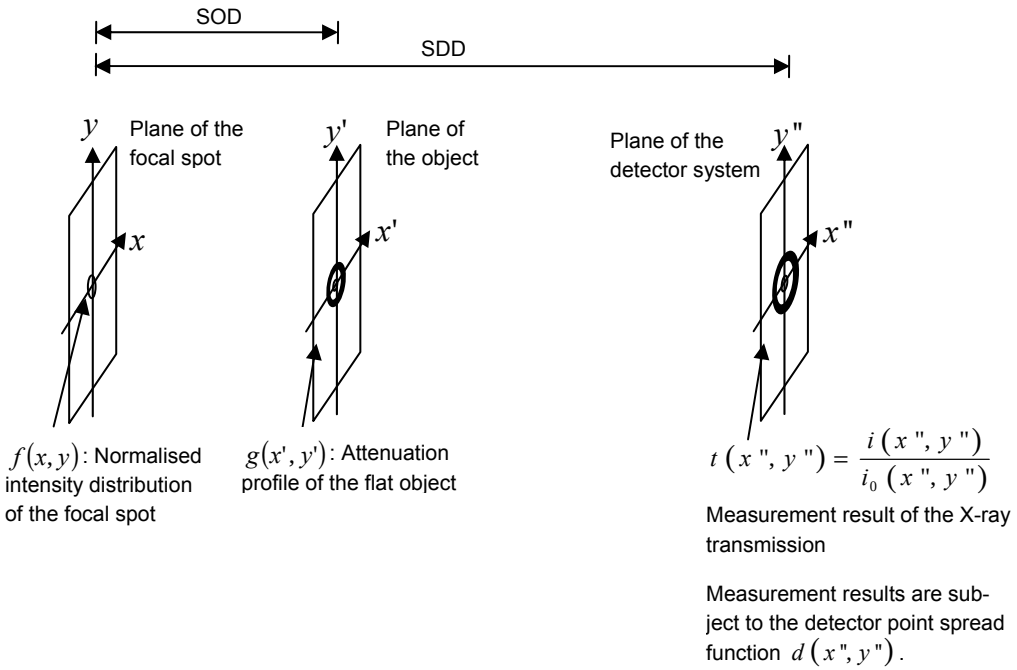

FIG. 1: Outline of the setup assumed.

The measurement result is estimated to be:

$$\underbrace{t(x",y")}_{\substack{\text{measurement result of the}\\ \text{x-ray transmission}}} = \underbrace{f(x,y)}_{\substack{\text{intensity distribution}\\ \text{of the focal spot}}} \otimes \underbrace{g(x',y')}_{\substack{\text{attenuation profile}\\ \text{of the flat object}}} \otimes \underbrace{d(x",y")}_{\substack{\text{detector point}\\ \text{spread function}}} + \underbrace{n(x",y")}_{\text{noise}} \tag{1}$$

$$= f\left(\frac{-x"}{V-1},\frac{-y"}{V-1}\right) \otimes g\left(\frac{x"}{V},\frac{y"}{V}\right) \otimes d(x",y") + n(x",y")$$

where:

- V is the geometrical magnification of the setup. It is calculated to be the distance between the source and the detector system (*SDD*) divided by the distance between the source and the object (*SOD*): $V = SDD/SOD$.
- (x,y), (x',y'), $(x",y")$ are the variables of the different coordinate systems.
- $\otimes$ is the mathematical convolution operation.
- $t(x",y")$ is the result of a measurement of the transmission of the X-ray beam through the flat test object.
- $f(x,y)$ is the intensity distribution of the focal spot.
- $g(x',y')$ is the transmission profile of the flat object.
- $d(x'',y'')$ is the pre-sampling point spread function of the detector system.
- $n(x",y")$ is the noise term.

No brackets are required in Eq. (1). The convolution operation is associative and commutative.

2.2 The Novel Approach

To a certain extent, image blurring which can be characterised by a convolution process can be removed using image deconvolution algorithms. According to Eq. (1), using the corresponding approximations and representing all functions in the same coordinate system, whereby the physical magnification effects are observed, a deconvolution of t with $g \otimes d$ yields an estimate of f.

This technique could be classified into the same group as [4], [5] and [6]. For these techniques, a suitable test object is measured. The resulting image corresponds to a convolution of the test object with the intensity distribution of the focal spot and other factors. Information on the focal spot is derived from this measurement using knowledge on the test object and other influencing values which means that the convolution process is undone to a certain extent. In contrast to [5] and [6], where certain assumptions are made on the shape of the focal spot and the measurement is accomplished in one dimension, with the presented method an arbitrary two dimensional intensity distribution can be measured.

2.3 Image Deconvolution Algorithms

In order to improve clarity, functions depending on two spatial coordinates (e. g. x'' and y'') are represented using lower case letters and the corresponding Fourier transforms depending on two spatial frequencies (e.g. u'' and v'') are represented using the corresponding capital letters, mostly without denomination of the arguments of the functions. According to the convolution theorem, a convolution in the spatial domain corresponds to a point-by-point multiplication in the corresponding Fourier domain. Furthermore, according to the addition theorem, an addition in the spatial domain corresponds to an addition in the corresponding Fourier domain. Using these theorems, Eq. (1) is rewritten to:

$$t = f \otimes p + n \Leftrightarrow T = F \cdot P + N \,, \tag{2}$$

where

- p is the point spread function (PSF) for the measurement of f. It is introduced in order to combine the transmission profile of the flat object g and the pre-sampling PSF of the detector system d: $p = g \otimes d$.
- T, F, P, and N are the complex Fourier transforms of these variables. It is assumed here, that T, F, P and N exist. $|P|$ is called modulation transfer function (MTF).

If the noise term was not present in this equation and $P \neq 0$ for all spatial frequencies, deconvolution could be accomplished using a simple division in Fourier space, e.g. $F = T/P$. This is referred to as an inverse filter. However, these assumptions are not valid for this application and for most other applications. Therefore, the inverse filter cannot be applied here. At certain spatial frequencies $|N|$ can be significantly higher than $|F \cdot P|$. At these spatial frequencies division of T by P mainly increases noise and deteriorates the image quality. This is due to the fact, that information on F is lost at these spatial frequencies. For that reason, independently of the deconvolution method applied, all spatial frequencies (in all directions) which are contained with high intensity in $|F|$ should be contained with high intensity in $|P|$ in order that $|F \cdot P|$ is significantly larger than $|N|$ for these spatial frequencies. This means that the test object (in combination with the detector imaging properties) should contain the major spatial frequencies which are required to describe the focal spot with sufficient intensity. In this case F can be restored well at these spatial frequencies, which yields a good estimate of f.

2.3.1 Deconvolution Using a Linear Filter

Various methods can be applied in order to avoid excessive noise amplification. A common approach is to multiply T with:

$$\frac{P^*}{|P|^2 + C}, \tag{3}$$

where the asterisk * stands for the complex conjugate and C can be a constant or a function of the spatial frequencies. If $C(u,v)$ is a function of the spatial frequencies *u* and *v*, which is calculated to be:

$$C(u,v) = \frac{\left\langle |N(u,v)|^2 \right\rangle}{\left\langle |F(u,v)|^2 \right\rangle}, \tag{4}$$

whereby the squared brackets $\langle\ \rangle$ are ensemble averages, Eq. (3) is called Wiener filter [8]. This filter minimises the mean squared error between the ideal image and the deblurred image, if the noise contained in the measurement data is Gaussian distributed and independent of the measurement data itself. In many practical applications C cannot be calculated according to Eq. (4) because $\left\langle |F(u,v)|^2 \right\rangle$ and $\left\langle |N(u,v)|^2 \right\rangle$ are not known. In this case *C* must be estimated. A rough estimation of *C* is accomplished in this paper using:

$$C \approx \alpha \frac{\int\int dx\ dy\ n(x,y)^2}{\int\int dx\ dy\ f(x,y)^2}, \tag{5}$$

whereby α is a user defined constant, which can be considered as a correction factor, and *n* and *f* are offset free. The numerator $\int\int dx\ dy\ n(x,y)^2$ can be estimated using the standard deviation of the grey values of several pixels for which the attenuation due to the object is almost identical. The denominator is approximated using a rough estimate of the intensity distribution of the focal spot.

2.3.2 Deconvolution Using Iterative Algorithms

Besides linear filters like the Wiener filter a great variety of image deconvolution algorithms exists. An overview can be found in Jansson et al. [8]. For the method described in the present paper, besides a linear filter, the Richardson Lucy maximum likelihood algorithm was applied. This algorithm makes use of further knowledge about the result namely the non-negativity of the deblurred image. Like many other modern deconvolution methods the Richardson Lucy maximum likelihood algorithm optimises a first guess of the deblurred image iteratively by convolving it with the point spread function *p* and comparing the result with the desired result *t*. For the simulations and measurements presented in this paper an accelerated version of the Richardson Lucy algorithm was applied.

It has been shown that, if this algorithm converges, it converges to the maximum likelihood solution for noise which follows Poisson counting statistics. For a discrete detector pixel raster this means that the standard deviation of the grey value of a pixel of *t* must be proportional to the square root of the expectation of this grey value in order that the algorithm eventually converges to the maximum likelihood solution. This is for example the

case if the grey values of *t* are proportional to the number of counts and noise present in *t* is only due to statistical fluctuations of the number of counted photons.

3. Simulations and Discussion of Sources of Measurement Errors

3.1. Scaling of the Grey Values of the Measurement Result and the Calculated Attenuation Profile

The differences between maximum and minimum transmission through the test object, which is called attenuation signal here, and the offset of the minimum transmission from zero transmission are scaled for the test object function blurred by the detector *p* and eventually also for the transmission image *t*. This is accomplished such that significant information is not lost due to rounding. For a real experiment *t* is measured and *p* is calculated and it is hardly possible to scale the attenuation signal and the offset in the same manner for *p* and *t*. For a theoretical point of view, in which the images are noise free, this scaling has no fundamental influence on the resulting focal spot *f*. Scaling the attenuation signal differently for *p* and *t* yields a certain scaling of the derived intensity distribution *f* of the focal spot. Eq. (2) is rewritten to $(\alpha_t \cdot t) = (\alpha_f \cdot f) \otimes (\alpha_p \cdot p)$, where α_t and α_p are scaling factors for *t* and *p,* respectively, and $\alpha_f = \alpha_t / \alpha_p$ is the corresponding scaling factor for *f*. This correlation can be proven by simple algebraic calculations using the definition of the convolution. If an offset o_p is added to the point spread function *p* and another offset o_t is added to the assumed measurement result *t*, the corresponding focal spot *f* has an (eventually negative) offset o_f : $(\alpha_t \cdot t + o_t) = (\alpha_f \cdot f + o_f) \otimes (\alpha_p \cdot p + o_p)$. This correlation can be proven and o_f can be calculated by Fourier transforming this equation and considering only the DC term. It is only valid, if the corresponding convolution exists.

However, the scaling of the offset and the attenuation signal of *t* and *p* can strongly influence image deconvolution algorithms. An offset o_f of the focal spot can influence a non-negativity constraint on the focal spot derived imposed by a deconvolution algorithm like the Richardson Lucy algorithm. Such a non-negativity constraint can limit fluctuations of the focal spot derived which are due to noise in *t*. If the expectation of the focal spot *f* has an offset, this effect is reduced. Furthermore, the scaling of the offset and the attenuation signal of *t* can influence assumptions made on the properties of noise which is present in *t*. For example, in order that the Richardson Lucy algorithm eventually converges to the maximum likelihood solution, the standard deviation of the grey value of a pixel of *t* must be proportional to the square root of the expectation of this grey value.

These effects will be taken into account for the following simulations and measurements.

3.2. Sampling

Unlike the theoretical calculations outlined above simulations and measurements are accomplished for a discrete pixel raster. The physical sampling process can be described mathematically using two operations. Firstly, the continuous image is convolved with the aperture function of a pixel. Each point of the resulting blurred image corresponds to the average of a surrounding area with the size of a detector pixel. Secondly, the blurred image is multiplied with an array of delta functions which are at the positions of the pixels.

The calculations used to derive the test object function blurred by the detector system *p* reproduce the physical sampling process to a high accuracy. The attenuation of the X-ray beam due to the test object is calculated along straight lines originating at the point-

like focal spot and ending at certain points of the detector system. These points form a point raster which is finer than the pixel raster of the detector system. The result is convolved with the (rescaled pre-sampling) detector point spread function *d* and then binned appropriately, which yields *p.* In this manner, the convolution with the aperture function of the pixel is reproduced to a high accuracy and pixels which are only partly covered by the shadow of the test object are accounted for.

Due to the sampling process, details of an image with a spatial frequency corresponding to a wavelength shorter than two pixels cannot be distinguished from details of the image with another specific spatial frequency. This effect is called aliasing. For that reason it is important, that the pixel raster of the detector system is sufficiently fine. A pixel raster for which the smallest line of the test pattern corresponds to approximately three pixels is considered to be sufficiently fine, because in this case the Fourier transforms of the simulated test patterns have very low values for spatial frequencies which cause aliasing.

3.3. Measurement Data which is Deteriorated by Noise

Because the transmission image *t* is deteriorated by noise, a perfect determination of the focal spot intensity distribution *f* is not possible. How accurately *f* can be determined from *t* depends in particular on the signal to noise ratio of *t* and on the shape of the test pattern applied. This was studied by means of simulations. The parameters of these simulations were chosen such that these simulations resemble the measurements presented in this paper as good as possible. The size of the acquired images was assumed to be 1024 x 1024 pixels.

As outlined above, all spatial frequencies which are contained with high intensity in the Fourier transform *F* of the intensity distribution of the focal spot should be contained with high intensity in the Fourier transform *P* of the test object blurred by the detector system, in order to be able to derive a good estimate of *f.* Simulations using various test objects were performed. For the measurements and simulations presented here, a ring pattern was chosen, because it fulfils these requirements very well. It has the shape of a Fresnel zone plate. Fresnel zone plates are often applied to focus X-rays. However, for the technique presented in this paper, the focussing properties are not made use of. Transmission measurements were simulated and performed. The boundaries of the rings are at radii $r_n = r_0 \cdot \sqrt{n}$ from the centre, where r_0 is the innermost radius and *n* is the number of the boundary. The ring pattern applied here has 80 boundaries. It contains spatial frequencies up to a line width of 3 detector pixels with high intensity in all directions.

It is assumed, that the pre-sampling point spread function (PSF) of the detector system *d* corresponds to a normal distribution with a standard deviation of 0.75 pixels. In order to reproduce the physical sampling process by the simulations the test patterns were simulated and convolved with *d* using a 4096 x 4096 pixel grid and then binned appropriately yielding simulated test objects blurred by the detector system *p*.

It is assumed that *f* corresponds to a normal distribution with a standard deviation of 3.5 detector pixels (independently of the magnification factor) which was cut off at two sides at a distance of the standard deviation from the centre and an oblique angle to the edges of the pixels, as shown in Fig. 2. The idealised images of the test objects are convolved with *f.* The results correspond to idealised noise free measurement results *t* in Eq. (2).

Furthermore noise is to be added to the blurred test objects yielding simulated measurement results *t.* It is assumed that the attenuation of the X-ray beam by the test objects is very low and that noise due to dark current and readout of the detector system is of a similar level for most pixels of the detector system. In this case, noise present in the measurement results is virtually the same for most pixels. In addition, the noise of the ac-

quired images is assumed to be “white”, which means that it is of equal intensity for all spatial frequencies contained in the image. These are realistic assumptions for the measurements presented in this paper. Based on these assumptions, noise is simulated by adding a random number with expectation zero and a standard deviation of 1/20, 1/10, 1/5 or 1/2.5 of the height of the attenuation signal for large structures to each pixel of the simulated blurred test objects. The contrast to noise ratio (CNR) is defined as the ratio between a certain attenuation signal and the standard deviation of the noise present in an image. The corresponding results have a CNR for large structures of 20, 10, 5 and 2.5, respectively. They are shown in Fig. 3 (top line).

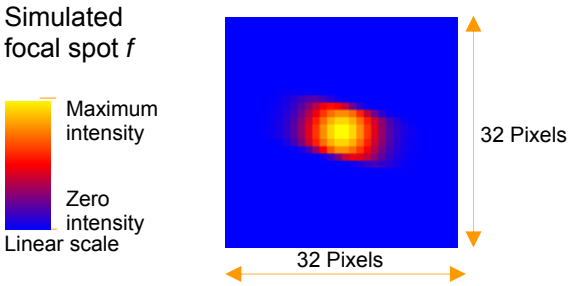

FIG. 2: Simulated focal spot intensity distribution f

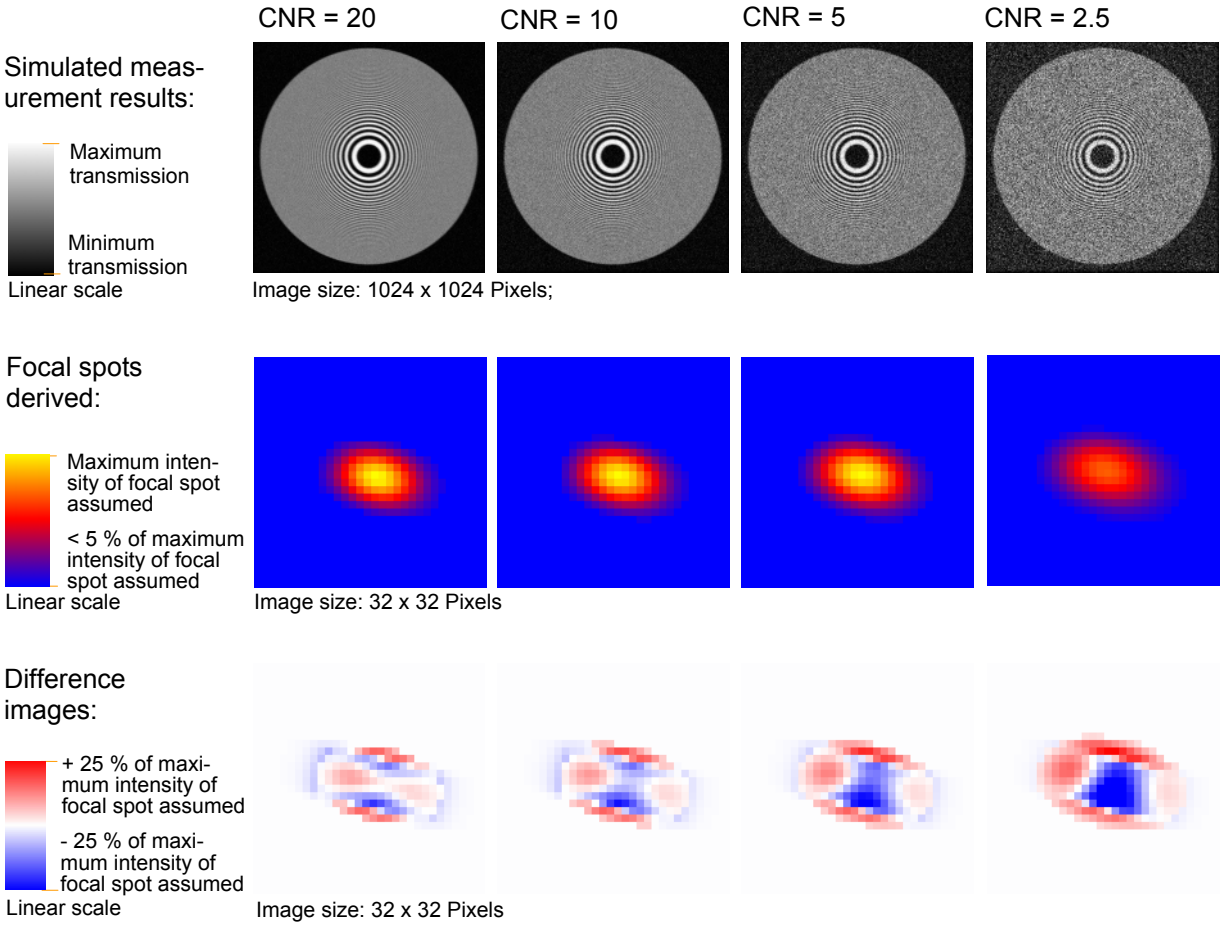

FIG. 3: Results of simulated transmission measurements of the ring pattern with a CNR of 20, 10, 5 and 2.5, focal spots derived from these simulated measurements using the Wiener filter according to Eq. (3) and Eq. (4) and difference images showing the deviation from the focal spot assumed.

First of all the Wiener filter was applied for deconvolution. For the application presented in the present paper, this filter is not influenced by the scaling of the offset and the attenuation signal of t and p, as long as the CNR is kept constant and $C(u,v)$ is calculated or estimated using the rescaled data. Grey values of the focal spots derived, which are smaller than 5 % of the maximum grey value, are set to zero and the total intensity of the resulting focal spot is normalized. The focal spots derived from the simulated transmission measurement results using the Wiener filter according to Eq. (3) and Eq. (4) and corresponding difference images are shown in Fig. 3. For a high CNR of t the results match the focal spot assumed well. As the CNR of t is lowered, deviations from the focal spot assumed are slightly increased. For these simulations, $C(u,v)$ was calculated according to Eq. (4), whereby $\langle |F(u,v)| \rangle$ and $\langle |N(u,v)| \rangle$ must be known. However, normally $\langle |F(u,v)| \rangle$ is not known for a real experiment and C must be estimated. For that reason, the focal spots derived from simulated measurements shown above represent best case results. For real experiments, C can be estimated using Eq. (5). Further simulations were accomplished in order to determine how strongly the estimate of C influences the result of the deconvolution. They show, that for a high CNR it is rather easy to estimate a reasonable value for the constant C, because a relatively large interval of values yields a good result, which strongly resembles the best case result (i.e. an interval of values which differ by up to a factor of 10 for a CNR of 20). However, for a low CNR only a small interval of values for C yields a reasonable result.

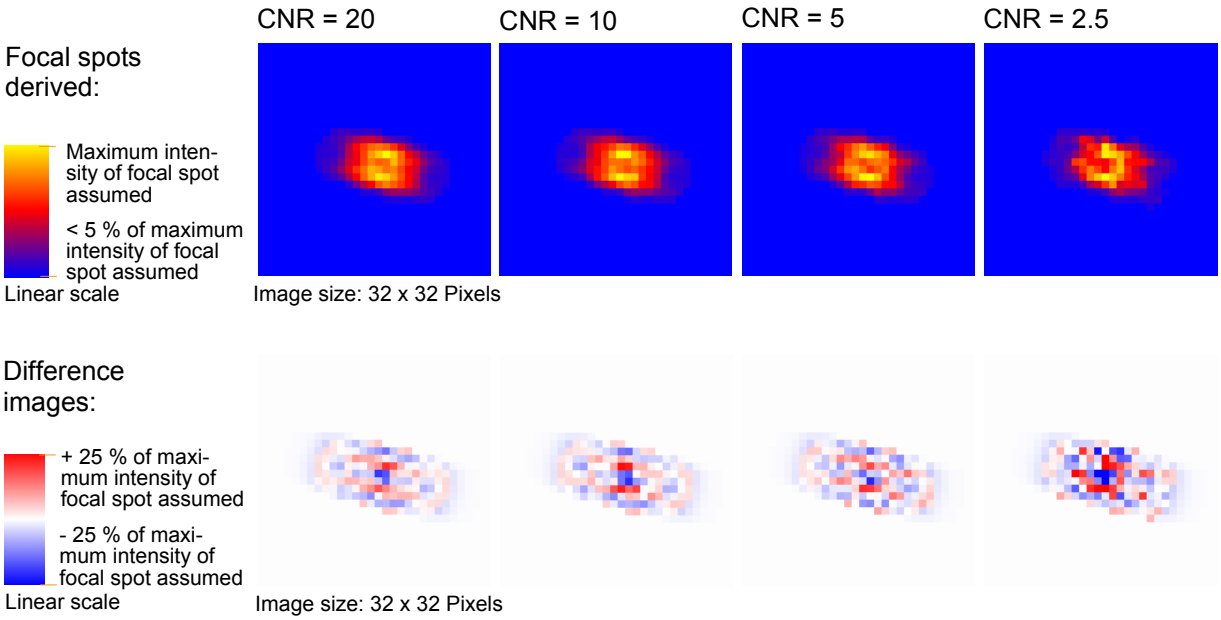

FIG. 4: Focal spots derived from simulated transmission measurements of the ring pattern with a CNR of 20, 10, 5 and 2.5 using the Richardson Lucy algorithm and difference images showing the deviation from the focal spot assumed.

In a second step, the measurement results, which were simulated as described above, were evaluated using the Richardson Lucy algorithm. For this algorithm the scaling of the attenuation signal and the offset of t strongly influences the result of the deconvolution. In order that the Richardson Lucy algorithm eventually converges to the maximum likelihood solution, the standard deviation of the grey value of a pixel of t must be proportional to the square root of the expectation of this grey value. For the simulations presented in this paper, the noise present in the (simulated) measurement results is the same for all

pixels. This is taken into account here by scaling the offset and the attenuation signal for t such that the offset is relatively large compared to the attenuation signal, as it would be the case for a real measurement result for which the attenuation due to the test object is low. According to Jansson et al. [8] this kind of noise could also be taken into account by using a slightly modified iteration. The offsets of t and p were scaled such that the corresponding focal spot f has an offset. In this manner, the effect of the non-zero constraint is reduced. Simulations with different test patterns using a wide range of different numbers of iterations were accomplished. Based on these simulations, for this application a number of 500 iterations is considered to be well sufficient to derive a good result, because the result is not influenced strongly, if the number of iterations is varied around 500 by a few hundreds. If a very high number of iterations is used instead, the result is not improved but becomes noisier.

The intensity distributions of the focal spots derived from the simulated transmission measurement results shown in Fig. 3 (top line) using the Richardson Lucy algorithm with 500 iterations and corresponding difference images are shown in Fig. 4. As for the Wiener filter, the results match the focal spot assumed less well for a lower CNR. The results are similar, but noisier and sharper compared to the results which were derived using the Wiener filter.

3.4. Geometrical Deviations of the Real Test Object from the Attenuation Profile Assumed

A thinkable source of systematic errors is a simulated attenuation profile g of the test object which does not match the real test pattern applied geometrically. In the simplest case the structures of g and t are shifted against each other. This yields a shifted focal spot intensity distribution f which is not of matter here.

However, if the geometry of the structures of g deviates significantly from the geometry of the structures of the transmission image t due to experimental inaccuracies, the focal spot intensity distribution f derived from the measurement will be wrong. This can have various reasons. The physical magnification factor V of the setup applied must be determined precisely in order that the attenuation profile g of the test object can be calculated correctly. This is also true for the rotation angle of the test object. However, a determination of this angle can be avoided by applying a rotationally symmetric pattern, e.g. a ring pattern. To a certain accuracy, the surface of the flat test object must be parallel to the surface of the detector system. However, an angle between the planes of the flat test object and the detector system which is sufficiently small, that the magnification factor does not vary significantly for different positions of the test object could as well be determined and taken into account by the simulations. Furthermore, the test object applied must have the shape assumed to a high accuracy.

These effects will be taken into account for the following measurements.

4. Measurements

The focal spot of a microfocus X-ray tube with a transmission target (phoenix|x-ray Systems + Services GmbH, XS 160 T-NF) was investigated for an acceleration voltage of 50 kV and a current of 60 μA, corresponding to 3 *Watts* target power. In order to avoid extra focal radiation, a copper plate with a hole of a diameter of approx. 0.5 *mm* at the position of the focal spot was placed onto the outside of the X-ray window.

The ring pattern used for the simulations shown above was applied as a test pattern. In order to be able to measure focal spots of various sizes, several samples of different size were produced. This was accomplished by Paul Scherrer Institut (PSI), Switzerland, using

electron beam lithography and reactive ion etching of a molybdenum layer on a 250 μm thick silicon substrate. The molybdenum structures applied have a depth of 1.4 μm. For the tube settings used for the experiments presented in this paper, a ring pattern with an inner radius of 32 μm, which yields a radius of the largest ring of approx. 286 μm and a smallest line width of 1.8 μm was chosen. The geometrical properties of the test patterns were verified using secondary electron microscopy (SEM). For the sample applied, only small deviations from the shape assumed, on the order of 10 % of the smallest line width, were observed, which should not cause significant measurement errors.

As a detector system a Perkin Elmer RID 1620 AJ with 2048 x 2048 pixels of 200 μm size was applied. For these measurements a region of 1024 x 1024 pixels was used. The pre-sampling detector point spread function (PSF) d was determined using a sharp copper edge, which was mounted directly onto the detector system, rotated by an angle of approximately five degrees in relation to the edges of the detector pixels.

A magnification factor of approx. 345 was chosen. In this case, the smallest line of the test object is projected onto approx. 3 pixels, which can be assumed to be sufficient to keep measurement errors due to aliasing low.

To a certain accuracy, the surface of the flat test object must be parallel to the surface of detector system. For this measurement a parallelism to an accuracy of $\pm 0.4°$ has been estimated. Using simple geometric calculations it can be shown, that this yields a maximum deviation of the test object function blurred by the detector system p from the transmission image t of less than approx 200 nm corresponding to 11 % of the smallest line width of the test sample applied, which should not cause significant measurement errors.

In order to determine the attenuation profile of the test object g, the attenuation of an appropriate X-ray spectrum due to the test object is calculated along straight lines originating at a point like focal spot and ending at different points of the surface of the detector system. These points form a point raster which is four times finer than the pixel raster of the detector system. The result is convolved with the (rescaled pre-sampling) detector PSF d. Then the result is binned appropriately, which yields p. These calculations reproduce the physical sampling process to a high accuracy. Using cross correlation of t and g the congruency of these two functions can be determined. With an optimisation algorithm the precise physical magnification factor can be determined to a very high accuracy by varying it, such that the maximum value of the result of the cross correlation is as high as possible. This works best, if the grey values of t and g are scaled such that the mean grey values of these two functions equal zero. For the measurements presented here, the optimisation algorithm converges to an accuracy corresponding to a deviation of the structures of p from the structures of t of less than 1 % of the smallest line of the test object, which can be assumed to be sufficient to keep measurement errors low. In order to calculate p, g is finally calculated for the precise magnification factor and convolved with d. These calculations are also accomplished using a pixel raster, which is four times finer than the pixel raster of the detector system and binned appropriately afterwards.

Three independent measurements were accomplished for which the same tube and detector settings were applied. The number of images used to determine t was varied, yielding total exposure times (for the measurement of i, i_0 and the corresponding offset) of approx. 3, 13 and 51 minutes. Fig. 5 shows the corresponding results which have contrast to noise ratios (CNRs) for large structures of about 5, 11 and 21. Because of the limited thickness of the structures of only 1.4 μm the attenuation of the X-ray beam due to the structures of the test object was only approx. 3 %.

At first, deconvolution was accomplished using a linear filter according to Eq. (3) and Eq. (5). The constant C was approximated using Eq. (5), whereby $\alpha \approx 0.1$ was chosen. In the same manner as for the simulations described above, the focal spots derived were set

to zero at values which are smaller that 5 % of the maximum value. Then the total intensities of the focal spots derived are normalised. The results are shown in Fig. 5.

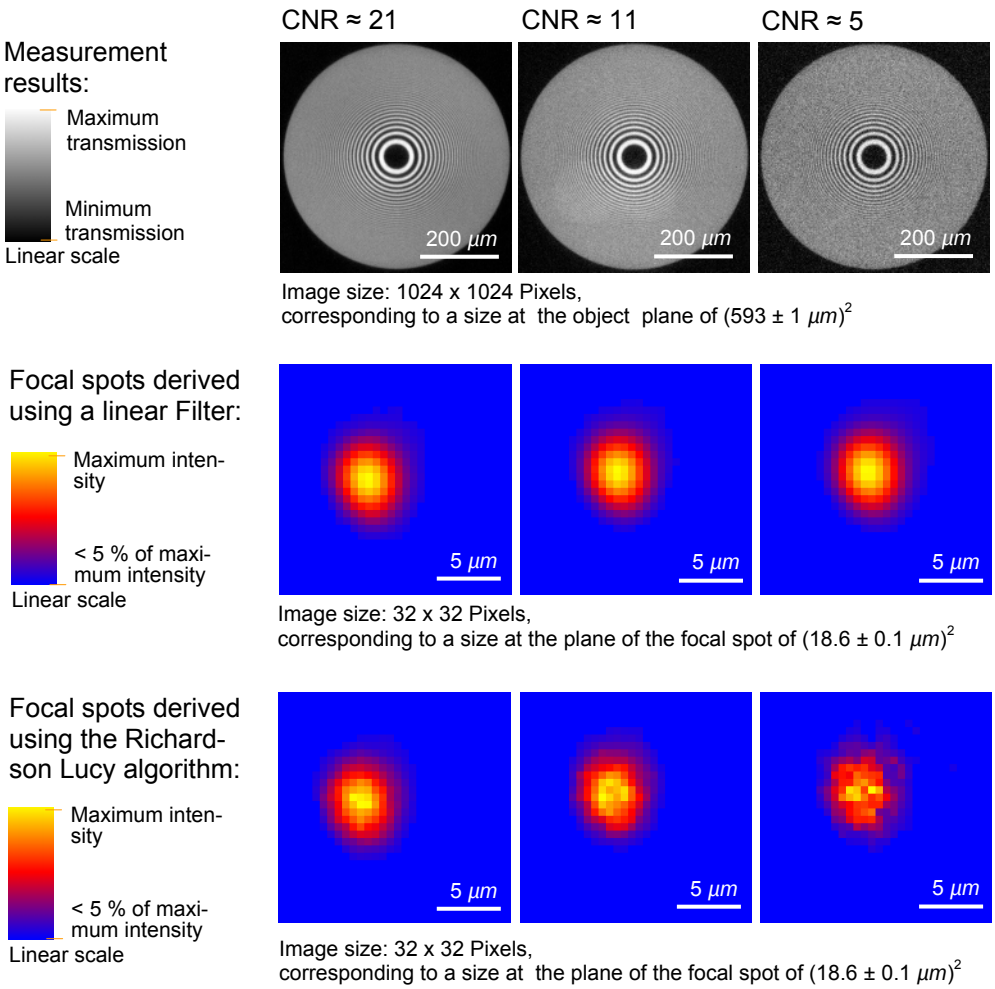

FIG. 5: Results of transmission measurements of the ring test pattern for three independent measurements with different total exposure times yielding contrast to noise ratios of 21, 11 and 5, focal spots derived using a linear filter according to Eq. (3) and Eq. (5) which is similar to the Wiener filter and focal spots derived using the Richardson Lucy algorithm with 500 iterations. The X-ray tube was operated at 50 kV and 60 µA. One pixel corresponds to 0.58 ± 0.5 µm of the focal spot and the test object, respectively.

Secondly, deconvolution was accomplished using the Richardson Lucy algorithm. In order that this algorithm eventually converges to the maximum likelihood solution, the offset of t must be high compared to the attenuation signal of t. This is the case for the measurement data. However, the offset of the measurement data had to be reduced in order to speed up the convergence of the algorithm. As for the simulations presented, the offsets and attenuation signals of t and p were scaled such that f has an offset, which reduces the effect of the non-negativity constraint of the Richardson-Lucy algorithm. In the same manner as the focal spots derived using a linear filter, the focal spots derived using the Richardson Lucy algorithm were set to zero at low values and then normalised. The results are shown in Fig. 5. The focal spot derived has a similar size and shape for all measurements and both algorithms. If the Richardson Lucy algorithm is applied, the focal spots derived become noisy if the contrast to noise ratio (CNR) of the transmission measurement is low.

For a target power of 3 Watts, the size of the focal spot is often assumed to be approximately 3 μm. The measured intensity of X-ray emission has dropped significantly (by approx 30 %) at a distance of 1.5 μm from the centre of the focal spot, which is sufficient to make structures of an object of less than 3 μm visible.

5. Conclusion and Outlook

It was shown that, under the conditions outlined above, it is possible to derive an image of the focal spot of a microfocus X-ray tube from a measurement of a suitable test object using a linear filter or the Richardson Lucy algorithm.

Besides the algorithms presented, other sophisticated deconvolution algorithms can be considered as well. A promising example is a commercially available maximum entropy deconvolution algorithm, described by Gull et al. [9]. This algorithm yields information on the accuracy of the deblurred images which might be used to determine error bars for the derived intensity maps of the focal spots.

It should be mentioned that the determination of the intensitiy distribution of the focal spot – as shown here – can be used to improve the quality of X-ray images based on image deconvolution algorithms. In this case the functions f (intensitiy distribution of the focal spot) and g (the attenuation profil of the object) invert the parts: f is known and g is unknown. The principles of calculation are therefore similar. This approach will be outlined in a succeeding paper.

Acknowledgements

First of all, we are very thankful to Dr. K. Jefimovs and Dr. C. David from PSI for the production of the test objects applied. Furthermore we want to thank A. Reinhold, the managing director of Feinfocus, for supplying another test object which was applied for first measurements and our collegues Dr. L. Bätz, P. Klofac, Dr. M. Goldammer, J. Stephan, and S. Krimmel for valuable assistance with technical and theoretical issues.

References

[1] International Electrotechnical Commission (IEC): “IEC Publication No. 336: X-ray tube assemblies for medical diagnosis-Characteristics of focal spots”, 3rd ed. IEC, Geneva, 1993

[2] National Electrical Manufacturers Association (NEMA): “NEMA Standard Publication No, XR-5: Measurement of Dimensions and Properties of Focal Spots of Diagnostic X-Ray Tubes”, NEMA, Washington DC, 1993

[3] Deutsches Institut für Normung (DIN): “DIN EN 12543“, Part 1-5, Beuth Verlag, Berlin, 1991

[4] J. Baumann, „Bestimmung des Fokusdurchmessers von Mikrofokus-Röntgenquellen mit Hilfe von Röntgen-Litographiemasken“, Poster, DGZfP Jahrestagung 1984, Deutsche Gesellschaft für zerstörungsfreie Prüfung (DGZfP), 1984, Essen

[5] U. Taubenreuther, Korrektur- und Kalibrierverfahren für die Kegelstrahl-(Mikro-)CT, Dissertation, Friedrich-Alexander-Universität Erlangen-Nürnberg, 2002

[6] A. Jobst, G. Kostka and P. Schmitt, “Neue Methode zur Charakterisierung von Brennflecken kleiner als 5 µm“, DACH Jahrestagung 2004, Deutsche Gesellschaft für zerstörungsfreie Prüfung (DGZfP), Salzburg, www.ndt.net, 2004

[7] H. H. Barrett and W. Swindell, Eds., Radiological Imaging. New York: Academic Press, 1981.

[8] P. A. Jansson, Ed., Deconvolution of Images and Spectra, Second Edition. New York: Academic Press, 1997.

[9] S.F. Gull and J. Skilling, Quantified Maximum Entropy MemSys5 User’s Manual, Version 1.2, Maximum Entropy Data Consultants Ltd., Suffolk, U.K., http://www.maxent.co.uk, 1999